J. Fluid Mech. (2022), *vol*. 938, A3, doi:10.1017/jfm.2022.116

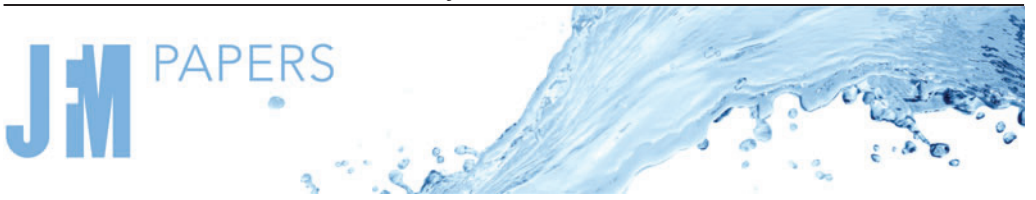

The effect of particle geometry on squirming through a shear-thinning fluid

Brandon van Gogh[1], Ebru Demir[2], D. Palaniappan[3] and On Shun Pak[1,†]

[1]Department of Mechanical Engineering, Santa Clara University, Santa Clara, CA 95053, USA

[2]Department of Mechanical Engineering and Mechanics, Lehigh University, Bethlehem, PA 18015, USA

[3]Department of Mathematics and Statistics, Texas A&M University–Corpus Christi, Corpus Christi, TX 78412, USA

(Received 14 August 2021; revised 11 January 2022; accepted 31 January 2022)

Biological and artificial microswimmers often encounter fluid media with non-Newtonian rheological properties. In particular, many biological fluids such as blood and mucus are shear-thinning. Recent studies have demonstrated how shear-thinning rheology can impact substantially the propulsion performance in different manners. In this work, we examine the effect of geometrical shape upon locomotion in a shear-thinning fluid using a prolate spheroidal squirmer model. We use a combination of asymptotic analysis and numerical simulations to quantify how particle geometry impacts the speed and the energetic cost of swimming. The results demonstrate the advantages of spheroidal over spherical swimmers in terms of both swimming speed and energetic efficiency when squirming through a shear-thinning fluid. More generally, the findings suggest the possibility of tuning the swimmer geometry to better exploit non-Newtonian rheological behaviours for more effective locomotion in complex fluids.

Key words: micro-organism dynamics

1. Introduction

Locomotion of microorganisms plays vital roles in various biological processes, including reproduction, foraging and biofilm formation (Fauci & Dillon 2006; Lauga 2016). Artificial microswimmers that move like their biological counterparts also show great promise for different biomedical applications such as drug delivery and microsurgery (Nelson, Kaliakatsos & Abbott 2010; Sengupta, Ibele & Sen 2012; Li *et al.* 2017). For their fundamental biological importance and potentially transformative applications, there have been growing interdisciplinary efforts in recent years to better understand the locomotion of these biological and artificial microswimmers (Moran & Posner 2017; Hu, Pané

† Email address for correspondence: opak@scu.edu

& Nelson 2018; Wu *et al.* 2020; Tsang *et al.* 2020*a*). These microswimmers employ a variety of mechanisms to overcome the dominance of viscous over inertial forces for self-propulsion at low Reynolds numbers. Extensive studies have shed light on the hydrodynamics of swimming microorganisms (Lauga & Powers 2009; Yeomans, Pushkin & Shum 2014; Elgeti, Winkler & Gompper 2015), which has also contributed to the development of various biomimetic or bioinspired artificial swimmers (Bente *et al.* 2018; Fu *et al.* 2021). More recently, there has also been a growing interest in exploring the application of machine learning in designing artificial microswimmers (Colabrese *et al.* 2017; Schneider & Stark 2019; Cichos *et al.* 2020; Tsang *et al.* 2020*b*; Hartl *et al.* 2021; Liu *et al.* 2021; Muiños-Landin *et al.* 2021).

Many microorganisms utilize one or more flexible appendages called flagella and cilia (short flagella) for locomotion. For instance, some spermatozoa of eukaryotic cells swim by propagating bending waves travelling along their flagellum. Colonies of flagellates such as *Volvox* (Goldstein 2015) and ciliates such as *Paramecium* and *Tetrahymena* have their surface covered by arrays of cilia beating in a coordinated manner. Lighthill (1952) and Blake (1971) first studied ciliary propulsion with the squirmer model, where the motion of closely packed cilia tips is represented by distribution of slip velocities on a spherical squirmer surface. In addition to representing specific ciliated microorganisms, the distribution of slip velocity can be adjusted to present different types of swimmers. Based on the representation by Lighthill (1952) and Blake (1971), the slip velocity is decomposed into a series of Legendre polynomials, where the coefficients of the series are associated with Stokes flow singularity solutions (Ghose & Adhikari 2014; Pak & Lauga 2014; Pedley 2016). The first mode of the decomposition corresponds to a source dipole and accounts for the swimming of the organism, and the second mode corresponds to a force dipole that characterizes the type of the swimmer. Many studies considered these two squirming modes to represent pushers and pullers, which obtain their thrust from, respectively, the rear (e.g. *Escherichia coli*) and front (e.g. *Chlamydomonas*) part of their body. The squirmer model has therefore become a widely used generic locomotion model for various problems in low-Reynolds-number swimming, including nutrient uptake by microorganisms (Magar, Goto & Pedley 2003; Magar & Pedley 2005; Michelin & Lauga 2011; Eastham & Shoele 2020), optimization (Michelin & Lauga 2010), hydrodynamic interactions (Ishikawa, Simmonds & Pedley 2006; Drescher *et al.* 2009), collective motion (Ishikawa & Pedley 2007; Ishikawa, Simmonds & Pedley 2007), inertial effects (Wang & Ardekani 2012; Chisholm *et al.* 2016) and swirling motion (Pedley, Brumley & Goldstein 2016; Binagia *et al.* 2020; Nganguia *et al.* 2020; Housiadas 2021; Housiadas, Binagia & Shaqfeh 2021), among others (Pedley 2016).

Of particular recent interest is the use of the squirmer model to probe the impact of non-Newtonian rheology on swimming (Zhu *et al.* 2011; Zhu, Lauga & Brandt 2012; Montenegro-Johnson, Smith & Loghin 2013; De Corato, Greco & Maffettone 2015; Datt *et al.* 2015; Binagia *et al.* 2020; Housiadas *et al.* 2021). Most biological fluids display non-Newtonian rheological behaviours, including viscoelasticity and shear-thinning viscosity. While extensive studies focused on the effect of fluid elasticity (Elfring & Lauga 2015; Sznitman & Arratia 2015; Li, Lauga & Ardekani 2021), recent studies have revealed how shear-thinning rheology can also affect locomotion in substantial and non-trivial ways (Lauga 2015; Montenegro-Johnson 2017). The impact of shear-thinning rheology varies among different types of swimmers and the details of their swimming gaits: while the propulsion speed of undulatory (Vélez-Cordero & Lauga 2013; Gagnon, Keim & Arratia 2014; Li & Ardekani 2015; Gagnon & Arratia 2016) and helical (Gómez *et al.* 2017; Demir *et al.* 2020; Qu & Breuer 2020) swimmers can be enhanced significantly,

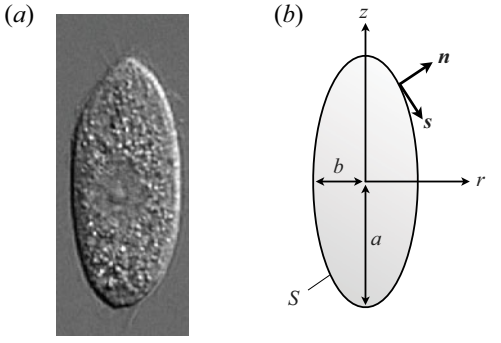

Figure 1. (*a*) An image of ciliate *Tetrahymena thermophila*. Image courtesy of Brian Bayless, Santa Clara University/Bayless Lab. (*b*) The geometrical set-up of a squirmer with a prolate spheroidal body, where a and b are, respectively, the semi-major and semi-minor axes. The unit normal $\boldsymbol{n} = \boldsymbol{e}_\tau$ and tangent $\boldsymbol{s} = -\boldsymbol{e}_\zeta$ vectors to the spheroidal surface S are expressed in terms of the basis vectors in the prolate spheroidal coordinates.

all two-mode squirmers (pushers, pullers or neutral squirmers) swim slower in a shear-thinning fluid (Montenegro-Johnson *et al.* 2013; Datt *et al.* 2015); it is noteworthy that speed enhancement is possible for squirmers with other squirming modes in the slip velocity (Datt *et al.* 2015; Pietrzyk *et al.* 2019). In addition, shear-thinning rheology can render ineffective swimming gaits in a Newtonian fluid (e.g. reciprocal motion) useful in a non-Newtonian fluid (Qiu *et al.* 2014; Han *et al.* 2020). Collectively, these studies demonstrate the profound impact of shear-thinning rheology on low-Reynolds-number locomotion.

In this work, we extend the spherical squirmer model to examine the effect of particle geometry on swimming in a shear-thinning fluid. While the squirmer model by Lighthill (1952) and Blake (1971) may be adequate for spherically shaped organisms like *Volvox*, swimmers with non-spherical shapes are commonly found in nature. To better represent ciliates such as *Paramecium* and *Tetrahymena* (see figure 1*a*) and, more generally, to probe the effect of geometrical shape upon ciliary locomotion, Keller & Wu (1977) generalized the squirmer model to a prolate spheroidal body of arbitrary eccentricity. The theoretical prediction of streamlines in their spheroidal model found good agreement with experimental streak photographs of freely swimming and inert sedimenting *Paramecium caudatum*. The original spheroidal squirmer model by Keller & Wu (1977) includes only the swimming mode without a force-dipole mode, which has been incorporated into the model by more recent studies (Ishimoto & Gaffney 2013; Theers *et al.* 2016; Pöhnl, Popescu & Uspal 2020) to represent other types of swimmers. In addition to representing ciliates with spheroidal bodies, the spheroidal model serves as a first approximation to other non-spherical swimmers (e.g. *E. coli*) to assess how geometrical shape affects swimming performance. Here, we extend the analysis to the non-Newtonian regime and probe the role of particle geometry on swimming in a shear-thinning fluid via the spheroidal squirmer model. A combined theoretical and numerical framework is used to quantify the impact on both the speed and the energetic cost of swimming. The results reveal key features that are distinct from the spherical case, suggesting the possibility for biological and artificial microswimmers to tune their geometrical shape for improving their swimming performance in complex fluids.

This paper is organized as follows. We formulate the problem in § 2 by introducing the prolate spheroidal squirmer model, the governing equations, and the rheological constitutive model employed in this work. In § 3, we present the asymptotic analysis

and numerical simulations used to quantify the locomotion of a spheroidal squirmer in a shear-tinning fluid. Results on the swimming speed, power dissipation and swimming efficiency, as well as their implications for the design of artificial microswimmers, are discussed in § 4. Finally, we conclude this work with closing remarks in § 5.

2. Problem formulation

2.1. *Geometrical set-up*

We use a spheroidal squirmer model to examine the effect of geometrical shape on locomotion in a shear-thinning fluid. Since many ciliates such as *Paramecium* and *Tetrahymena* have prolate spheroidal bodies (see figure 1*a*), we focus on the locomotion of a prolate spheroidal squirmer in this work for its biological relevance. See figure 1(*b*) for notations and geometrical set-up. The equation describing the surface of the prolate spheroidal body reads

$$\frac{z^2}{a^2} + \frac{r^2}{b^2} = 1, \tag{2.1}$$

where $r^2 = x^2 + y^2$, a is the semi-major axis, and $b \leq a$ is the semi-minor axis. The spheroidal coordinate system that we use is given by (τ, ζ, ϕ), where $1 \leqslant \tau \leqslant \infty$, $-1 \leqslant \zeta \leqslant 1$ and $0 \leqslant \phi \leqslant 2\pi$. The position vector is given by

$$\boldsymbol{x} = c\sqrt{\tau^2 - 1}\sqrt{1 - \zeta^2}\,\boldsymbol{e}_r + c\tau\zeta\,\boldsymbol{e}_z, \tag{2.2}$$

where $\boldsymbol{e}_r = \cos\phi\,\boldsymbol{e}_x + \sin\phi\,\boldsymbol{e}_y$, $c = \sqrt{a^2 - b^2}$ is half of the focal length, and $e = c/a$ is the eccentricity. Here, we define $\tau_0 = 1/e$, with $\tau > \tau_0$ corresponding to the fluid domain exterior to the surface ($\tau = \tau_0$) of the squirmer. The unit vectors of the prolate spheroidal coordinates $\boldsymbol{e}_\tau$ and $\boldsymbol{e}_\zeta$ are related to those of the Cartesian coordinates as

$$\boldsymbol{e}_\tau = \frac{\tau\sqrt{1-\zeta^2}}{\sqrt{\tau^2-\zeta^2}}\,\boldsymbol{e}_r + \frac{\zeta\sqrt{\tau^2-1}}{\sqrt{\tau^2-\zeta^2}}\,\boldsymbol{e}_z, \quad \boldsymbol{e}_\zeta = -\frac{\zeta\sqrt{\tau^2-1}}{\sqrt{\tau^2-\zeta^2}}\,\boldsymbol{e}_r + \frac{\tau\sqrt{1-\zeta^2}}{\sqrt{\tau^2-\zeta^2}}\,\boldsymbol{e}_z. \tag{2.3a,b}$$

The metric coefficients for the prolate spheroidal coordinates are given by

$$h_\tau = c\,\frac{\sqrt{\tau^2-\zeta^2}}{\sqrt{\tau^2-1}}, \quad h_\zeta = c\,\frac{\sqrt{\tau^2-\zeta^2}}{\sqrt{1-\zeta^2}}, \quad h_\phi = c\sqrt{1-\zeta^2}\sqrt{\tau^2-1}. \tag{2.4a–c}$$

The unit normal and tangent vectors on the spheroidal surface are given by the basis vectors, respectively, as $\boldsymbol{n} = \boldsymbol{e}_\tau$ and $\boldsymbol{s} = -\boldsymbol{e}_\zeta$.

2.2. *The squirmer model*

Similar to the spherical squirmer model (Lighthill 1952; Blake 1971), surface velocities are prescribed on a prolate spheroidal squirmer to represent the effect of the ciliary motion on the fluid. Following Keller & Wu (1977), a steady tangential velocity distribution of the form $\boldsymbol{u}^S = -B_1(\boldsymbol{s}\cdot\boldsymbol{e}_z)\boldsymbol{s}$ is prescribed on the squirmer surface S (figure 1*b*). In the spherical limit, $\boldsymbol{s} \to \boldsymbol{e}_\theta$, and the squirming velocity reduces to the first mode $\boldsymbol{u}^S = B_1 \sin\theta\,\boldsymbol{e}_\theta$ considered by Lighthill (1952) and Blake (1971). Subsequent studies have included additional modes of surface velocities (Ishimoto & Gaffney 2013; Theers *et al.* 2016;

Eastham & Shoele 2020; Pöhnl *et al.* 2020). In particular, Theers *et al.* (2016) included the contribution of a force-dipole as a second mode (B_2) in the form

$$\boldsymbol{u}^S = -B_1(\boldsymbol{s}\cdot\boldsymbol{e}_z)\boldsymbol{s} - B_2\zeta(\boldsymbol{s}\cdot\boldsymbol{e}_z)\boldsymbol{s} \tag{2.5}$$

$$= -B_1\tau_0(1+\alpha\zeta)\sqrt{\frac{1-\zeta^2}{\tau_0^2-\zeta^2}}\,\boldsymbol{e}_\xi, \tag{2.6}$$

where the sign of the ratio $\alpha = B_2/B_1$ represents a pusher ($\alpha < 0$) or puller ($\alpha > 0$), and the case $\alpha = 0$ corresponds to a neutral squirmer. The two-mode spheroidal squirmer reduces to the spherical model by Lighthill (1952) and Blake (1971) in the limit of zero eccentricity ($e = 0$). Here, we extend previous analyses on spherical squirmers in a shear-thinning fluid (Montenegro-Johnson *et al.* 2013; Datt *et al.* 2015) and examine the effect of particle geometry via the spheroidal squirmer model given by (2.6).

2.3. *Governing equations*

The momentum and continuity equations in the limit of low Reynolds number are, respectively, given by

$$\nabla\cdot\boldsymbol{\sigma} = \boldsymbol{0}, \tag{2.7}$$

$$\nabla\cdot\boldsymbol{u} = 0, \tag{2.8}$$

where $\boldsymbol{\sigma} = -p\boldsymbol{I} + \boldsymbol{T}$, p is the pressure, $\boldsymbol{I}$ is the identity tensor, and $\boldsymbol{T}$ is the deviatoric stress tensor. To capture the reduction in the viscosity due to increased shear rates in a shear-thinning fluid, we use the Carreau constitutive equation (Bird, Armstrong & Hassanger 1987), where

$$\boldsymbol{T} = [\mu_\infty + (\mu_0 - \mu_\infty)(1+\lambda^2|\dot{\boldsymbol{\gamma}}|^2)^{(n-1)/2}]\dot{\boldsymbol{\gamma}}. \tag{2.9}$$

Here, μ_0 and μ_∞ are, respectively, the zero and infinite shear rate viscosities, and the strain rate tensor $\dot{\boldsymbol{\gamma}} = \nabla\boldsymbol{u} + (\nabla\boldsymbol{u})^{\mathrm{T}}$ has magnitude $|\dot{\boldsymbol{\gamma}}| = (\dot{\gamma}_{ij}\dot{\gamma}_{ij}/2)^{1/2}$. The power-law index $n < 1$ characterizes the degree of shear-thinning, and $1/\lambda$ characterizes the critical shear rate at which the non-Newtonian behaviour becomes significant. The Carreau model has been shown to be effective in describing the rheological behaviours of different biological fluids, and has been employed in previous studies of locomotion in a shear-thinning fluid (Montenegro-Johnson *et al.* 2013; Vélez-Cordero & Lauga 2013; Datt *et al.* 2015; Li & Ardekani 2015; Nganguia *et al.* 2020).

In the laboratory frame, the flow decays to zero in the far field

$$\boldsymbol{u}(\tau\to\infty,\zeta) = \boldsymbol{0}, \tag{2.10}$$

and the boundary condition on the surface of the squirmer is given by

$$\boldsymbol{u}(\tau=\tau_0,\zeta) = \boldsymbol{u}^S + \boldsymbol{U}, \tag{2.11}$$

where the squirming velocity distribution $\boldsymbol{u}^S$ given by (2.6) causes the squirmer to translate with an unknown swimming velocity $\boldsymbol{U}$. The system is closed by enforcing the force-free condition

$$\int_S \boldsymbol{n}\cdot\boldsymbol{\sigma}\,\mathrm{d}S = \boldsymbol{0}, \tag{2.12}$$

where $\boldsymbol{n} = \boldsymbol{e}_\tau$ is the unit normal vector on the squirmer surface. We note that the axisymmetric velocity distribution in (2.6) does not induce any rotational velocity and the squirmer is torque-free. By symmetry, swimming occurs in the z-direction, $\boldsymbol{U} = U\boldsymbol{e}_z$.

We non-dimensionalize the problem by scaling lengths by a, velocities by B_1, strain rates by $\omega = B_1/a$, and stresses by $\mu_0\omega$. The dimensionless momentum and continuity equations are given by, respectively, $\nabla \cdot \boldsymbol{\sigma}^* = \mathbf{0}$ and $\nabla \cdot \boldsymbol{u}^* = 0$, where the stars (*) denote dimensionless variables. The deviatoric stress tensor $\boldsymbol{T}^*$ takes a dimensionless form

$$\boldsymbol{T}^* = [\beta + (1-\beta)(1 + Cu^2|\dot{\boldsymbol{\gamma}}^*|^2)^{(n-1)/2}]\dot{\boldsymbol{\gamma}}^*, \tag{2.13}$$

where the Carreau number $Cu = \omega\lambda$ compares the characteristic strain rate ω to the critical strain rate $1/\lambda$, and the viscosity ratio $\beta = \mu_\infty/\mu_0$ compares the zero and infinite shear rate viscosities. Both dimensionless groups measure the extent of the shear-thinning effect. Hereafter we refer only to dimensionless variables and therefore drop the stars for convenience.

3. Asymptotic analysis and numerical simulations

3.1. *Asymptotic analysis*

The Carreau constitutive equation (2.13) reduces to the Newtonian constitutive equation when $Cu = 0$ or $\beta = 1$. We can therefore examine the weakly non-Newtonian behaviour by expanding variables in the limits of small Cu ($\varepsilon = Cu^2 \ll 1$) or small deviation of β from unity ($\varepsilon = 1 - \beta \ll 1$) in perturbation series

$$\{\boldsymbol{u}, \boldsymbol{\sigma}, \boldsymbol{T}, \dot{\boldsymbol{\gamma}}, U\} = \{\boldsymbol{u}_0, \boldsymbol{\sigma}_0, \boldsymbol{T}_0, \dot{\boldsymbol{\gamma}}_0, U_0\} + \varepsilon\{\boldsymbol{u}_1, \boldsymbol{\sigma}_1, \boldsymbol{T}_1, \dot{\boldsymbol{\gamma}}_1, U_1\} + O(\varepsilon^2). \tag{3.1}$$

The zeroth-order solution corresponds to the flow around a spheroidal squirmer in a Newtonian fluid, which satisfies

$$\nabla \cdot \boldsymbol{\sigma}_0 = \mathbf{0}, \tag{3.2}$$

$$\nabla \cdot \boldsymbol{u}_0 = 0, \tag{3.3}$$

where $\boldsymbol{\sigma}_0 = -p_0\boldsymbol{I} + \dot{\boldsymbol{\gamma}}_0$ and $\dot{\boldsymbol{\gamma}}_0 = \nabla\boldsymbol{u}_0 + (\nabla\boldsymbol{u}_0)^{\mathrm{T}}$. The boundary condition on the squirmer surface is given by $\boldsymbol{u}_0(\tau = \tau_0, \zeta) = \boldsymbol{u}^S + \boldsymbol{U}_0$, and the flow decays to zero in the far field. The Newtonian solution was obtained in previous analyses (Keller & Wu 1977; Theers *et al.* 2016; Pöhnl *et al.* 2020). In terms of streamfunction ψ_0 in prolate spheroidal coordinates, where

$$\boldsymbol{u}_0 = \frac{1}{h_\zeta h_\phi}\frac{\partial\psi_0}{\partial\zeta}\boldsymbol{e}_\tau - \frac{1}{h_\tau h_\phi}\frac{\partial\psi_0}{\partial\tau}\boldsymbol{e}_\zeta, \tag{3.4}$$

the solution is given by

$$\psi_0 = C_1 H_2(\tau) G_2(\zeta) + C_2\tau(1-\zeta^2) + C_3 H_3(\tau) G_3(\zeta) + C_4\zeta(1-\zeta^2), \tag{3.5}$$

where $G_n(x)$ and $H_n(x)$ are, respectively, the Gegenbauer functions of the first and second kind of degree $-1/2$, and the coefficients are determined as

$$\left.\begin{aligned} C_1 &= \frac{2U_0(\tau_0^2+1) - 4\tau_0^2}{\tau_0^2[(\tau_0^2+1)\coth^{-1}\tau_0 - \tau_0]}, \quad C_2 = \frac{\tau_0\left[\tau_0 - (\tau_0^2-1)\coth^{-1}\tau_0\right] - U_0}{\tau_0^2[(\tau_0^2+1)\coth^{-1}\tau_0 - \tau_0]}, \\ C_3 &= \frac{4\alpha}{\tau_0[3\tau_0 + (1-3\tau_0^2)\coth^{-1}\tau_0]}, \quad C_4 = \frac{\alpha\left[2/3 - \tau_0^2 + \tau_0(\tau_0^2-1)\coth^{-1}\tau_0\right]}{\tau_0[3\tau_0 + (1-3\tau_0^2)\coth^{-1}\tau_0]}. \end{aligned}\right\} \tag{3.6}$$

Upon enforcing the force-free condition (2.12), the swimming speed of a spheroidal squirmer in a Newtonian fluid is equal to (Keller & Wu 1977; Theers *et al.* 2016)

$$U_0 = \tau_0[\tau_0 - (\tau_0^2 - 1)\coth^{-1}\tau_0]. \tag{3.7}$$

At $O(\varepsilon)$, the momentum and continuity equations are, respectively, given by

$$\nabla \cdot \boldsymbol{\sigma}_1 = \mathbf{0}, \tag{3.8}$$

$$\nabla \cdot \boldsymbol{u}_1 = 0, \tag{3.9}$$

where $\boldsymbol{\sigma}_1 = -p_1\boldsymbol{I} + \boldsymbol{T}_1$ and the first non-Newtonian correction to the deviatoric stress is $\boldsymbol{T}_1 = \dot{\boldsymbol{\gamma}}_1 + \boldsymbol{A}$; here, the tensor $\boldsymbol{A}$ depends on the choice of the asymptotic limit, $\varepsilon = Cu^2$ or $\varepsilon = 1 - \beta$. Expanding (2.13) with $\varepsilon = Cu^2$ gives

$$\boldsymbol{A} = \frac{(1-\beta)(n-1)}{2}|\dot{\boldsymbol{\gamma}}_0|^2\dot{\boldsymbol{\gamma}}_0, \tag{3.10}$$

whereas expanding (2.13) with $\varepsilon = 1 - \beta$ gives

$$\boldsymbol{A} = \left[-1 + (1 + Cu^2|\dot{\boldsymbol{\gamma}}_0|^2)^{(n-1)/2}\right]\dot{\boldsymbol{\gamma}}_0. \tag{3.11}$$

We consider results in both asymptotic limits in the following sections.

To obtain the first non-Newtonian correction to the swimming speed $\boldsymbol{U}_1$, we use the Lorentz reciprocal theorem (Stone & Samuel 1996; Lauga 2014; Elfring 2017; Masoud & Stone 2019) to bypass solving (3.8) and (3.9) for the first-order flow, $(\boldsymbol{u}_1, p_1)$. To apply the reciprocal theorem, we consider an auxiliary Stokes flow problem of the same geometry, satisfying

$$\nabla \cdot \hat{\boldsymbol{\sigma}} = \mathbf{0}, \tag{3.12}$$

$$\nabla \cdot \hat{\boldsymbol{u}} = 0, \tag{3.13}$$

where $\hat{\boldsymbol{\sigma}} = -\hat{p}\boldsymbol{I} + \nabla\hat{\boldsymbol{u}} + (\nabla\hat{\boldsymbol{u}})^{\mathrm{T}}$. From (3.8) and (3.12), we take the inner products between the flow fields and the divergence of the stress fields in the auxiliary and first-order problems to obtain the relation

$$\hat{\boldsymbol{u}} \cdot (\nabla \cdot \boldsymbol{\sigma}_1) = \boldsymbol{u}_1 \cdot (\nabla \cdot \hat{\boldsymbol{\sigma}}) = 0. \tag{3.14}$$

With the identity $\hat{\boldsymbol{u}} \cdot (\nabla \cdot \boldsymbol{\sigma}_1) - \boldsymbol{u}_1 \cdot (\nabla \cdot \hat{\boldsymbol{\sigma}}) = \nabla \cdot (\hat{\boldsymbol{u}} \cdot \boldsymbol{\sigma}_1 - \boldsymbol{u}_1 \cdot \hat{\boldsymbol{\sigma}}) + (\nabla\boldsymbol{u}_1 : \hat{\boldsymbol{\sigma}} - \nabla\hat{\boldsymbol{u}} : \boldsymbol{\sigma}_1)$, we integrate (3.14) over the fluid volume and use the divergence theorem to obtain

$$\int_S \boldsymbol{n} \cdot \hat{\boldsymbol{\sigma}} \cdot \boldsymbol{u}_1 \,\mathrm{d}S - \int_S \boldsymbol{n} \cdot \boldsymbol{\sigma}_1 \cdot \hat{\boldsymbol{u}} \,\mathrm{d}S = \int_V \boldsymbol{\sigma}_1 : \nabla\hat{\boldsymbol{u}} \,\mathrm{d}V - \int_V \hat{\boldsymbol{\sigma}} : \nabla\boldsymbol{u}_1 \,\mathrm{d}V. \tag{3.15}$$

By substituting the expression of the stresses $\hat{\boldsymbol{\sigma}}$ and $\boldsymbol{\sigma}_1$ in the auxiliary and first-order problems into the right-hand side of (3.15), we obtain

$$\int_S \boldsymbol{n} \cdot \hat{\boldsymbol{\sigma}} \cdot \boldsymbol{u}_1 \,\mathrm{d}S - \int_S \boldsymbol{n} \cdot \boldsymbol{\sigma}_1 \cdot \hat{\boldsymbol{u}} \,\mathrm{d}S = \int_V \boldsymbol{A} : \nabla\hat{\boldsymbol{u}} \,\mathrm{d}V. \tag{3.16}$$

In order to determine $\boldsymbol{U}_1$, we choose the auxiliary Stokes flow problem to be the flow due to the translation of a prolate spheroid with velocity $\hat{\boldsymbol{U}}$ (Happel & Brenner 1965).

The relation (3.16) thus becomes

$$\hat{\boldsymbol{F}} \cdot \boldsymbol{U}_1 - \boldsymbol{F}_1 \cdot \hat{\boldsymbol{U}} = \int_V \boldsymbol{A} : \nabla \hat{\boldsymbol{u}} \, \mathrm{d}V, \tag{3.17}$$

where $\hat{\boldsymbol{F}} = \int_S \boldsymbol{n} \cdot \hat{\boldsymbol{\sigma}} \, \mathrm{d}S = -8\pi \hat{\boldsymbol{U}}/\tau_0[(\tau_0^2 + 1)\coth^{-1}\tau_0 - \tau_0]$ is the force experienced by a translating spheroid in the auxiliary problem. By enforcing the force-free condition (2.12) at $O(\varepsilon)$, $\boldsymbol{F}_1 = \int_S \boldsymbol{n} \cdot \boldsymbol{\sigma}_1 \, \mathrm{d}S = \boldsymbol{0}$, the reciprocal theorem gives the final result

$$\hat{\boldsymbol{F}} \cdot \boldsymbol{U}_1 = \int_V \boldsymbol{A} : \nabla \hat{\boldsymbol{u}} \, \mathrm{d}V, \tag{3.18}$$

where only two known Stokes flow solutions, namely the zeroth-order ($\boldsymbol{u}_0$) and auxiliary ($\hat{\boldsymbol{u}}$) problems, are required to determine the non-Newtonian swimming velocity $\boldsymbol{U}_1$.

In addition to the first-order swimming velocity, the reciprocal theorem can be applied to obtain the first-order power dissipation when considering the energetic cost of squirming through a shear-thinning fluid (Nganguia, Pietrzyk & Pak 2017), which we will examine in more detail in § 4.2.

3.2. *Numerical simulations*

To compare with the results from the asymptotic analysis, we also perform fully coupled numerical simulations of the momentum and continuity equations (2.7) and (2.8), together with the Carreau constitutive equation (2.9), using the finite element method implemented in the COMSOL Multiphysics environment. To take advantage of the axial symmetry of the problem, an axisymmetric computational domain in the r–z plane is used to simulate only half of the full flow domain. The squirmer is modelled as a half spheroid whose major axis coincides with the axis of symmetry. To simulate the locomotion of a squirmer in an unbounded fluid, we ensure that the computational domain (of size $500a \times 500a$) is sufficiently large so that the numerical results are independent of the size of the domain. We perform the simulations in a reference frame moving with the squirmer, which leads to a uniform flow in the far field as the inflow boundary condition. The magnitude of the inflow is equal to the unknown swimming speed of the squirmer, which is obtained by solving the momentum and continuity equations simultaneously, with the force-free swimming condition (2.12) as a global equation. A zero pressure is specified for the outflow boundary condition. P2 + P1 discretization is applied to the flow field: namely, second-order elements are used for the velocity components, and first-order elements are used for the pressure. Triangular mesh elements are used for the simulations, with local mesh refinement near the squirmer to resolve properly the spatial variation of the viscosity. The degrees of freedom are of the order of 1.8×10^5 for the simulations. We used PARDISO (the Parallel Direct Solver) for all simulations.

In addition to comparing with the asymptotic results in this work, we have validated our numerical implementation against previous results for both spherical (Lighthill 1952; Blake 1971) and spheroidal (Keller & Wu 1977; Theers *et al.* 2016) squirmers in a Newtonian fluid, as well as spherical squirmers in a shear-thinning fluid (Datt *et al.* 2015).

4. Results and discussion

4.1. *Swimming speed*

We use results from both the asymptotic analysis and numerical simulations to examine the effect of particle geometry on squirming through a shear-thinning fluid. We first

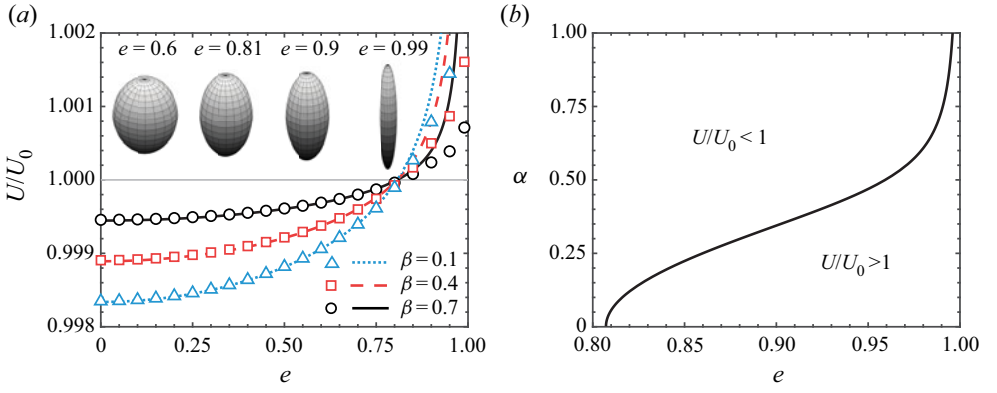

Figure 2. (*a*) Swimming speed of a spheroidal squirmer U in a shear-thinning fluid relative to its corresponding Newtonian value U_0 as a function of eccentricity e for different values of viscosity ratio β. Here, $\alpha = 0$, $n = 0.25$ and $Cu = 0.1$. Both asymptotic (lines) and numerical (symbols) results predict that enhanced swimming ($U/U_0 \geqslant 1$) occurs when the eccentricity exceeds a critical value $e_c \approx 0.81$. (*b*) For a pusher/puller ($\alpha \neq 0$), the α–e diagram maps the regimes where enhanced ($U/U_0 > 1$) and hindered ($U/U_0 < 1$) swimming occur.

consider the small Carreau number limit, $\varepsilon = Cu^2$, by substituting the expression (3.10) into (3.18) to obtain the swimming speed in a shear-thinning fluid as $U \sim U_0 + Cu^2 U_1$. The Newtonian speed U_0 is given by (3.7), and the first non-Newtonian correction reads

$$U_1 = \frac{(1-\beta)(n-1)}{2}\left[\sum_{i=0}^{3}\gamma_i(\tau_0) + \alpha^2\chi(\tau_0)\sum_{i=0}^{7}\delta_i(\tau_0)\right], \tag{4.1}$$

where $\gamma_i(\tau_0)$, $\delta_i(\tau_0)$ and $\chi(\tau_0)$ are constants depending on τ_0; their expressions are given in Appendix A. Figure 2(*a*) shows the results from the asymptotic analysis (lines) given by (4.1) and numerical simulations (symbols). The asymptotic result (4.1) reveals that the propulsion speed varies linearly with $1-\beta$ and $n-1$; in numerical simulations we set $n = 0.25$ for its relevance to biological mucus (Hwang, Litt & Forsman 1969; Vélez-Cordero & Lauga 2013). Previous studies (Montenegro-Johnson *et al.* 2013; Datt *et al.* 2015) found that cylindrical and spherical squirmers with the first two modes (pushers, pullers and neutral squirmers) swim consistently slower in a shear-thinning fluid ($U/U_0 < 1$). Interestingly, the asymptotic analysis reveals that it is possible for a spheroidal squirmer to swim faster in a shear-thinning fluid than in a Newtonian fluid ($U/U_0 > 1$; figure 2*a*): for a neutral squirmer ($\alpha = 0$), enhanced swimming occurs when $\sum_{i=0}^{3}\gamma_i(\tau_0) < 0$, which can be solved numerically to obtain a critical eccentricity, $e_c \approx 0.81$, above which a spheroidal squirmer swims at a speed higher than its Newtonian value, as shown in figure 2(*a*). For a pusher/puller ($\alpha \neq 0$), an increase in the magnitude of α acts to reduce the swimming speed in the small Cu limit. Figure 2(*b*) maps the regimes where enhanced ($U/U_0 > 1$) and hindered ($U/U_0 < 1$) swimming occur in this asymptotic limit. The critical value of α is determined from (4.1) as

$$\alpha_c = \sqrt{\frac{-\sum_{i=0}^{3}\gamma_i(\tau_0)}{\chi(\tau_0)\sum_{i=0}^{7}\delta_i(\tau_0)}}, \tag{4.2}$$

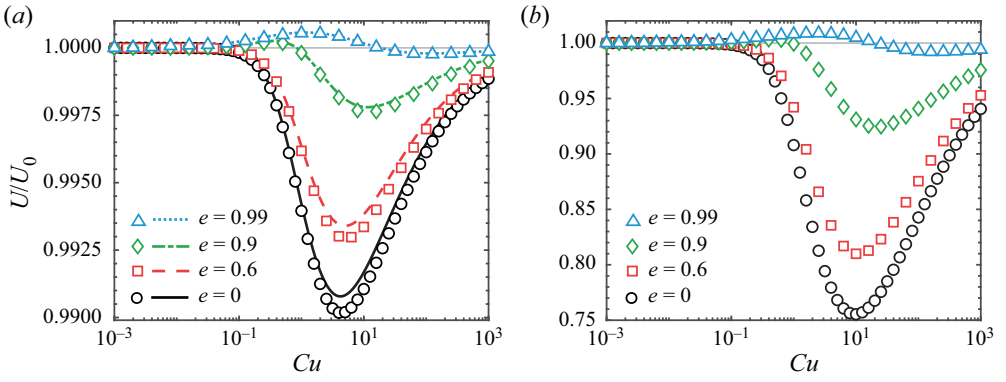

Figure 3. (*a*) Swimming speed of a spheroidal squirmer U in a shear-thinning fluid relative to its corresponding Newtonian value U_0 as a function of Cu for different values of eccentricity e when $\beta = 0.9$. The asymptotic results in the small $\varepsilon = 1 - \beta$ limit (lines) agree well with numerical simulations (symbols). An increased value of eccentricity enhances the swimming speed in general. For values of eccentricity above the critical value (e.g. $e = 0.9$ and 0.99), the squirmer can swim faster in a shear-thinning fluid than in a Newtonain fluid. The qualitative behaviours remain the same beyond the weakly non-Newtonian regime when $\beta = 0.1$ as shown by numerical simulations in (*b*); we also note the substantially larger speed variations in (*b*). In both (*a*,*b*), $\alpha = 0$ and $n = 0.25$.

for different values of the eccentricity (solid line, figure 2*b*). We note that the above result is independent of β and n, which appear only in the prefactor in the asymptotic expression (4.1). We also remark that the quadratic dependence on α in (4.1) shows that the swimming speed does not depend on the sign of α (i.e. a pusher versus a puller), which still holds beyond the asymptotic regime considered here, as shown by numerical simulations (see Appendix B for more details). While the sign of α does not affect the swimming speed, the detailed velocity and pressure fields surrounding a squirmer depend on both the magnitude and sign of α.

To examine the dependence of swimming speed over a full range of Cu, we consider the other asymptotic limit, $\varepsilon = 1 - \beta$, and use (3.11) in the integral theorem (3.18). Figure 3(*a*) displays different types of non-monotonic variations with Cu in this asymptotic limit, depending on the value of eccentricity. Here, we focus on the results for neutral squirmers ($\alpha = 0$); the results for pushers ($\alpha < 0$) and pullers ($\alpha > 0$) can be obtained in a similar fashion (see Appendix B). For a spherical squirmer ($e = 0$) and a spheroidal squirmer with an eccentricity below the critical value ($e = 0.6 < e_c$), the swimming speed first decays with increased Cu, reaching a local minimum before approaching the Newtonian value as Cu continues to increase. However, for squirmers with eccentricities above the critical value ($e > e_c \approx 0.81$; e.g. $e = 0.9$ and 0.99 in figure 3*a*), the speed first increases with Cu, attaining a local maximum speed that is faster than the corresponding Newtonian value before approaching the Newtonian value at larger values of Cu. We note that the seemingly minute variations are merely consequences of the use of small parameters in the asymptotic analysis. In figure 3(*b*) we verify through numerical simulations with $\beta = 0.1$ that these features remain the same beyond the weakly non-Newtonian regime; the speed variations are substantially larger compared with the asymptotic results. These results highlight the importance of particle geometry on swimming in a shear-thinning fluid: while shear-thinning rheology acts to retard the motion of a spherical squirmer, increasing the eccentricity (or slenderness) of the particle helps to mitigate the speed reduction generally; moreover, the speed could even be enhanced relative to the Newtonian

value at certain values of Cu when the eccentricity is above the critical value. In particular, it is noteworthy that a spheroidal squirmer with $e = 0.99$ has only relatively minute variations of swimming speed over a wide range of Cu, as shown in figure 3. This feature illustrates the possibility of designing a spheroidal swimmer that can restore effectively the substantial loss of swimming speed due to shear-thinning viscosity in the spherical case. Such a robust performance is especially desirable for swimmers that need to traverse complex media with vastly varying rheological properties.

In figure 4, we examine the distributions of flow speed, pressure and viscosity around a spheroidal squirmer with different eccentricities obtained by numerical simulations. As the eccentricity increases, the variations of flow speed (figure 4*a*), pressure (figure 4*b*) and viscosity (figure 4*c*) all become increasingly localized at the poles of the squirmer. In particular, the viscosity distributions in figure 4(*c*) provide some insights that may help us to understand the observed dependence of propulsion speed on the squirmer geometry. For a spherical squirmer, the viscosity reduction in a shear-thinning fluid is fairly uniform around the squirmer, as shown in figure 4(*c*) ($e = 0$). The physical scenario may therefore be akin to a squirmer immersed in a low-viscosity inner fluid surrounded by a high-viscosity outer fluid. Such a confinement effect was shown to reduce the propulsion speed of the squirmer (Reigh & Lauga 2017), consistent with the speed reduction of a spherical squirmer in a shear-thinning fluid. When the squirmer becomes more eccentric, the viscosity reduction becomes more non-uniform, with the reduction concentrating around the poles and diminished reduction near the equator. Such localization of viscosity reduction disrupts the uniform confinement effect in the spherical case, contributing plausibly to the increasingly restored propulsion speed in a shear-thinning fluid as the squirmer becomes more spheroidal. As shown in figure 4(*c*), the localization is particularly apparent for a highly eccentric squirmer ($e = 0.99$), which indeed can swim faster in a shear-thinning fluid than in a Newtonian fluid, in stark contrast to the case of a spherical squirmer.

As a remark, the (soft) confinement effect may have qualitatively different consequences on the propulsion of different types of swimmers. In particular, the enhanced propulsion of undulatory (Li & Ardekani 2015; Riley & Lauga 2017) and helical (Gómez *et al.* 2017; Demir *et al.* 2020) swimmers was attributed to the soft confinement effect, which could instead cause the speed reduction of a spherical squirmer (Reigh & Lauga 2017). The results on spheroidal squirmers here further illustrate how the effect may manifest differently depending on the particle geometry, highlighting this subtle and significant factor in understanding locomotion in a shear-thinning fluid.

4.2. *Power dissipation and swimming efficiency*

We next consider the effect of particle geometry on the energetic cost of squirming through a shear-thinning fluid. We calculate the power $\mathcal{P}$ expended by the squirmer during the swimming process, which is equal to the power dissipation in the fluid:

$$\mathcal{P} = -\int_S \boldsymbol{n}\cdot\boldsymbol{\sigma}\cdot\boldsymbol{u}\,\mathrm{d}S. \tag{4.3}$$

Here, we focus on results for a neutral squirmer; contributions from other modes can be calculated in a similar fashion. We expand $\mathcal{P}$ in the asymptotic limit of small ε,

$$\mathcal{P} = \mathcal{P}_0 + \varepsilon\mathcal{P}_1 + O(\varepsilon^2), \tag{4.4}$$

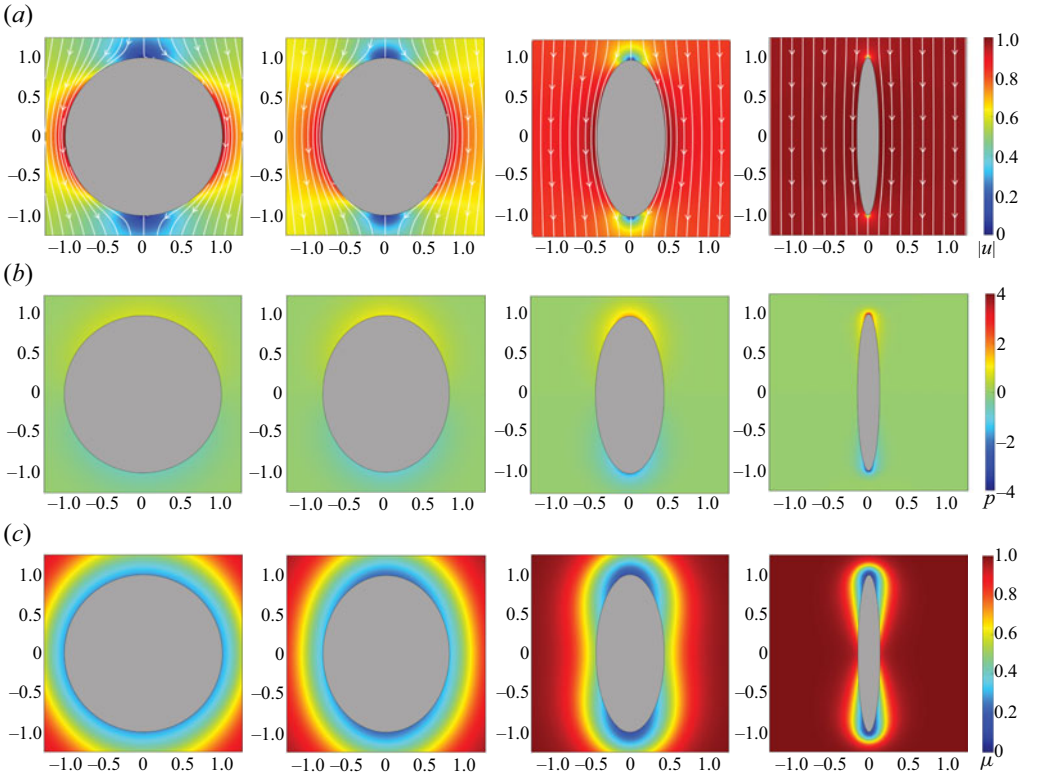

Figure 4. Distributions of (*a*) flow speed $|\boldsymbol{u}|$, (*b*) pressure p, and (*c*) viscosity μ around a spheroidal squirmer with different eccentricities in the co-moving frame in a shear-thinning fluid. From left to right, the eccentricity is $e = 0$, 0.6, 0.9 and 0.99. Here, $\alpha = 0$, $\beta = 0.1$, $Cu = 10^{0.4}$ and $n = 0.25$.

where the Newtonian power dissipation is given by Keller & Wu (1977) as

$$\mathcal{P}_0 = \frac{4\pi(\tau_0^2 - 1)\left[(1 + \tau_0^2)\coth^{-1}\tau_0 - \tau_0\right]}{\tau_0}, \tag{4.5}$$

and the first non-Newtonian correction is given by $\mathcal{P}_1 = -\int_S \boldsymbol{n}\cdot\boldsymbol{\sigma}_1\cdot\boldsymbol{u}_0\,\mathrm{d}S - \int_S \boldsymbol{n}\cdot\boldsymbol{\sigma}_0\cdot\boldsymbol{u}_1\,\mathrm{d}S$. By applying the boundary condition $\boldsymbol{u}_1 = \boldsymbol{U}_1$ on the squirmer surface, the second integral in $\mathcal{P}_1$ becomes $\int_S \boldsymbol{n}\cdot\boldsymbol{\sigma}_0\,\mathrm{d}S\cdot\boldsymbol{U}_1$, which vanishes due to the force-free condition $\int_S \boldsymbol{n}\cdot\boldsymbol{\sigma}_0\,\mathrm{d}S = \boldsymbol{0}$. The first non-Newtonian correction to the power dissipation is therefore given by

$$\mathcal{P}_1 = -\int_S \boldsymbol{n}\cdot\boldsymbol{\sigma}_1\cdot\boldsymbol{u}_0\,\mathrm{d}S. \tag{4.6}$$

We can again bypass the calculation of the first-order stress $\boldsymbol{\sigma}_1$ and obtain $\mathcal{P}_1$ via the reciprocal theorem (3.16) by choosing an appropriate auxiliary problem. Specifically, here we choose the auxiliary problem to be the zeroth-order (or Newtonian) flow around a spheroidal squirmer (Keller & Wu 1977): $(\hat{p}, \hat{\boldsymbol{u}}) = (p_0, \boldsymbol{u}_0)$. The integral relation (3.16) hence becomes

$$\int_S \boldsymbol{n}\cdot\boldsymbol{\sigma}_0\cdot\boldsymbol{u}_1\,\mathrm{d}S - \int_S \boldsymbol{n}\cdot\boldsymbol{\sigma}_1\cdot\boldsymbol{u}_0\,\mathrm{d}S = \int_V \boldsymbol{A}:\nabla\boldsymbol{u}_0\,\mathrm{d}V, \tag{4.7}$$

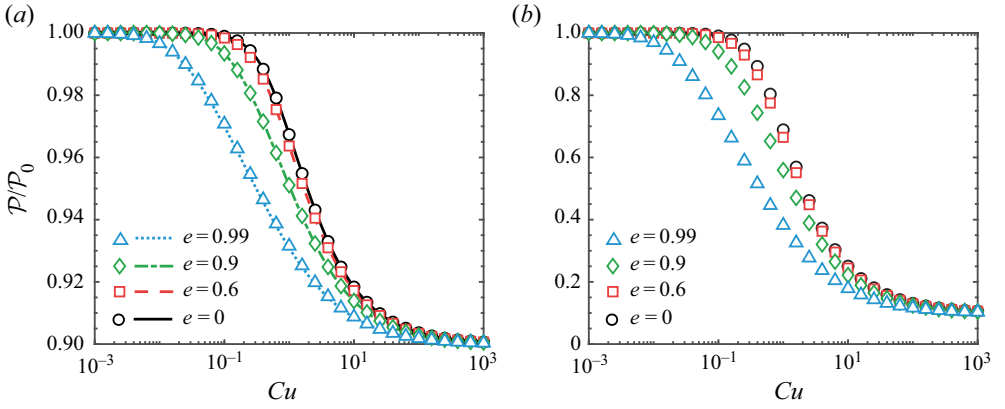

Figure 5. (*a*) Power dissipation of a spheroidal squirmer $\mathcal{P}$ in a shear-thinning fluid relative to its corresponding Newtonian value $\mathcal{P}_0$ as a function of Cu for different values of eccentricity e when $\beta = 0.9$. The asymptotic results in the small $\varepsilon = 1 - \beta$ limit (lines) agree well with numerical simulations (symbols). The qualitative behaviours remain the same beyond the weakly non-Newtonian limit when $\beta = 0.1$, as shown by numerical simulations in (*b*). In both (*a*,*b*), $\alpha = 0$ and $n = 0.25$. While the behaviours are qualitatively similar in (*a*,*b*), we note the substantially larger variations in (*b*).

where the first integral on the left-hand side vanishes, $\int_S \boldsymbol{n}\cdot\boldsymbol{\sigma}_0\cdot\boldsymbol{u}_1\,\mathrm{d}S = \int_S \boldsymbol{n}\cdot\boldsymbol{\sigma}_0\,\mathrm{d}S\cdot\boldsymbol{U}_1 = 0$, due to the boundary condition $\boldsymbol{u}_1 = \boldsymbol{U}_1$ on S and the force-free condition $\int_S \boldsymbol{n}\cdot\boldsymbol{\sigma}_0\,\mathrm{d}S = \boldsymbol{0}$. The reciprocal theorem therefore allows us to express (4.6) as (De Corato *et al.* 2015; Nganguia *et al.* 2017)

$$\mathcal{P}_1 = \int_V \boldsymbol{A} : \nabla\boldsymbol{u}_0\,\mathrm{d}V. \tag{4.8}$$

We use quadrature to calculate the power dissipation from (4.8) for a wide range of Cu in the small $\varepsilon = 1 - \beta$ limit. Figure 5(*a*) displays results from the asymptotic analysis and numerical simulations, which both show that the power dissipation decreases with Cu in general. In addition, an increased eccentricity further reduces the energetic cost of squirming through a shear-thinning fluid. We verify by numerical simulations that the same trends hold beyond the weakly non-Newtonian regime in figure 5(*b*).

Next, we use the power dissipation to calculate the efficiency of swimming through a shear-thinning fluid. Lighthill (1975) introduced the Froude efficiency, a concept borrowed from propeller theory, to characterize the efficiency of swimming at low Reynolds numbers. The swimming efficiency is defined as

$$\eta = \frac{\tilde{\mathcal{P}}}{\mathcal{P}}, \tag{4.9}$$

which compares the power expended by the squirmer swimming in the shear-thinning fluid, $\mathcal{P}$, to the power required to tow a particle of the same geometry at the same swimming speed, $\tilde{\mathcal{P}}$. The power in the towing problem is given by $\tilde{\mathcal{P}} = \tilde{\boldsymbol{F}}\cdot\boldsymbol{U}$, where $\tilde{\boldsymbol{F}}$ is the force required to tow a rigid spheroid at the swimming velocity $\boldsymbol{U}$ in the same shear-thinning fluid. We calculate the efficiency asymptotically (De Corato *et al.* 2015; Nganguia *et al.* 2017) as

$$\eta = \eta_0 + \varepsilon\eta_1 + O(\varepsilon^2). \tag{4.10}$$

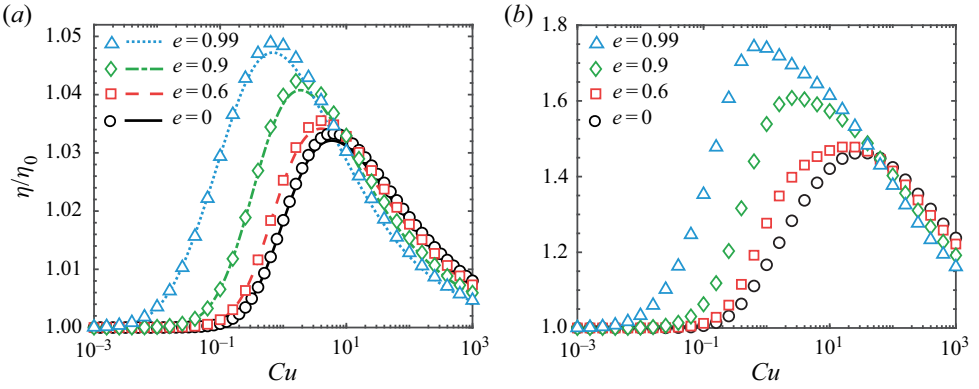

Figure 6. (*a*) Swimming efficiency of a spheroidal squirmer η in a shear-thinning fluid relative to its corresponding Newtonian value η_0 as a function of Cu for different values of eccentricity e when $\beta = 0.9$. The asymptotic results in the small $\varepsilon = 1 - \beta$ limit (lines) agree well with numerical simulations (symbols). The qualitative behaviours remain the same beyond the weakly non-Newtonian limit when $\beta = 0.1$, as shown by numerical simulations in (*b*). In both (*a*,*b*), $\alpha = 0$ and $n = 0.25$. While the behaviours are qualitatively similar in (*a*,*b*), we note the substantially larger variations in (*b*).

The zeroth-order (Newtonian) value is given by Keller & Wu (1977) as $\eta_0 = 2\tau_0^2[\tau_0 + (1-\tau_0^2)\coth^{-1}\tau_0]^2/(\tau_0^2-1)[\tau_0 - (1+\tau_0^2)\coth^{-1}\tau_0]^2$, and the first-order correction η_1 is calculated with asymptotic expansions of $\mathcal{P} \sim \mathcal{P}_0 + \varepsilon\mathcal{P}_1$ and $\tilde{\mathcal{P}} \sim \tilde{\mathcal{P}}_0 + \varepsilon\tilde{\mathcal{P}}_1$. The expansion of the towing power is given by

$$\tilde{\mathcal{P}} = \tilde{\boldsymbol{F}}_0 \cdot \boldsymbol{U}_0 + \varepsilon(\tilde{\boldsymbol{F}}_1 \cdot \boldsymbol{U}_0 + \tilde{\boldsymbol{F}}_0 \cdot \boldsymbol{U}_1) + O(\varepsilon^2), \tag{4.11}$$

which involves expansions of the swimming velocity $\boldsymbol{U} \sim \boldsymbol{U}_0 + \varepsilon\boldsymbol{U}_1$ and towing force $\tilde{\boldsymbol{F}} \sim \tilde{\boldsymbol{F}}_0 + \varepsilon\tilde{\boldsymbol{F}}_1$, where the first-order corrections to both quantities are again determined by the reciprocal theorem (Datt *et al.* 2015; Nganguia *et al.* 2017). Figure 6(*a*) displays the asymptotic results for swimming efficiency in the small $\varepsilon = 1 - \beta$ limit (lines), which agree well with results by full numerical simulations (symbols). First, the swimming efficiency is enhanced generally relative to the Newtonian case, $\eta/\eta_0 > 1$. Second, for a given eccentricity, there exists an optimal value of Cu that maximizes the swimming efficiency. Finally, the maximum swimming efficiency attainable increases with the eccentricity. We verify by numerical simulations that the same trends hold beyond the weakly non-Newtonian regime in figure 6(*b*); when the viscosity is $\beta = 0.1$, an eccentricity of $e = 0.99$ allows the swimming efficiency to be enhanced significantly by almost 80 % relative to the Newtonian efficiency in a shear-thinning fluid. We also remark that, unlike propulsion speed, there is no qualitative change in terms of propulsion efficiency below or above the critical eccentricity; the squirmer consistently propels more efficiently in a shear-thinning fluid for all eccentricities considered.

Overall, the asymptotic and numerical results presented here demonstrate that a spheroidal squirmer can swim both faster (§ 4.1) and more efficiently (this subsection) compared with its spherical counterpart in a shear-thinning fluid.

5. Conclusion

Biological and artificial microswimmers often need to traverse biological fluids with complex rheological properties. In particular, shear-thinning viscosity is a ubiquitous non-Newtonian fluid behaviour of many biological fluids, which can impact swimming

in substantial and non-trivial ways. Via a spherical squirmer model, previous works showed that shear-thinning viscosity can lead to substantial loss of swimming speed compared with swimming in a Newtonian fluid. In this work, we extend these previous analyses and consider a spheroidal squirmer to probe the effect of particle geometry on the performance of swimming in a shear-thinning fluid. Through asymptotic analysis and numerical simulations, our results show that by increasing its eccentricity, a spheroidal squirmer can effectively restore the loss of swimming speed in a shear-thinning fluid. Indeed, when the eccentricity exceeds a critical value, the spheroidal squirmer can swim faster in a shear-thinning fluid than in a Newtonian fluid, a feature in stark contrast to the corresponding cases of spherical squirmers. As a particular example, we demonstrate that a spheroidal squirmer with a large eccentricity can have a robust swimming performance over a wide range of Carreau numbers, a feature particularly desirable for swimmers that need to traverse environments with vastly varying properties. In addition to the swimming speed, the energetic cost of swimming through a shear-thinning fluid reduces with an increased eccentricity. The swimming efficiency of a spheroidal squirmer can be enhanced substantially as a result.

Taken together, the results here demonstrate the advantages of spheroidal over spherical swimmers in terms of locomotion performance in a shear-thinning fluid, which call for comparisons with future experiments with biological and artificial microswimmers. Recent studies have shed light on optimal swimming of non-spherical swimmers in a Newtonian fluid (Guo *et al.* 2021; Daddi-Moussa-Ider *et al.* 2021). The findings here suggest the possibility and hence opportunity of fine-tuning the swimmer geometry to better exploit non-Newtonian rheological behaviours for more effective locomotion in complex fluids.

Funding. We acknowledge the National Science Foundation for funding support under CBET-1931292 and EFMA-1830958 (to O.S.P.). Computations were performed using the WAVE computing facility at Santa Clara University, enabled by the Wiegand Foundation.

Declaration of interests. The authors report no conflict of interest.

Author ORCIDs.
Ebru Demir https://orcid.org/0000-0002-2099-1679;
On Shun Pak https://orcid.org/0000-0003-1510-7049.

Author contributions. B.v.G and E.D. contributed equally to this work.

Appendix A

In this appendix, we list the expressions for the constants in the swimming speed given by (4.1) in the small Carreau number limit. The constants associated with the B_1 squirming mode are given by

$$\gamma_0 = \frac{1}{\tau_0(\tau_0^2-1)}\sum_{k=0}^{7} D_k^0 \tau_0^{2k+1}, \tag{A1}$$

$$\gamma_1 = \frac{(\tau_0^2-1)\coth^{-1}\tau_0}{\tau_0}\sum_{k=0}^{6} D_k^1 \tau_0^{2k}, \tag{A2}$$

$$\gamma_2 = \frac{(\tau_0^2-1)^3(\coth^{-1}\tau_0)^2}{\tau_0}\sum_{k=0}^{1} D_k^2 \tau_0^{2k+6}, \tag{A3}$$

k	D_k^0	D_k^1	D_k^2	D_k^3
0	$-\frac{35}{128}$	$\frac{35}{128}$	$-\frac{9}{16}$	$\frac{9}{16}$
1	$\frac{85}{384}$	$\frac{15}{64}$	$-\frac{15}{2}$	$\frac{15}{2}$
2	$-\frac{107}{384}$	$\frac{67}{128}$	—	—
3	$\frac{31}{128}$	$\frac{103}{64}$	—	—
4	$\frac{713}{128}$	$-\frac{743}{128}$	—	—
5	$-\frac{30\,559}{1920}$	$-\frac{17}{8}$	—	—
6	$\frac{5801}{384}$	$\frac{613}{128}$	—	—
7	$-\frac{613}{128}$	—	—	—

Table 1. Values of D_k^i in the constants associated with the B_1 squirming mode given by (A1)–(A4).

$$\gamma_3 = \frac{\lambda(\tau_0^2-1)^3}{\tau_0}\sum_{k=0}^{1} D_k^3 \tau_0^{2k+6}, \tag{A4}$$

where $\lambda = Li_2[(1-\tau_0)/(1+\tau_0)] + \pi^2/12 - 2\ln[(2\tau_0)/(1+\tau_0)]\coth^{-1}\tau_0$, $Li_2(x)$ is the dilogarithm function of the variable x, and the values of D_k^i are given in table 1.

The constants associated with the B_2 squirming mode are given by

$$\chi = \frac{1}{\left[(3\tau_0^2-1)\coth^{-1}(\tau_0) - 3\tau_0\right]^2}, \tag{A5}$$

$$\delta_0 = \frac{1}{\tau_0^2-1}\sum_{k=0}^{5} E_k^0 \tau_0^{2k+4}, \tag{A6}$$

$$\delta_1 = \frac{\coth^{-1}\tau_0}{\tau_0^2-1}\sum_{k=0}^{6} E_k^1 \tau_0^{2k+3}, \tag{A7}$$

$$\delta_2 = \frac{(\coth^{-1}\tau_0)^2}{\tau_0^2-1}\sum_{k=0}^{14} E_k^2 \tau_0^{k+2}, \tag{A8}$$

$$\delta_3 = (\tau_0^2-1)(\coth^{-1}\tau_0)^3\sum_{k=0}^{12} E_k^3 \tau_0^{k+1}, \tag{A9}$$

$$\delta_4 = (\tau_0^2-1)^2(\coth^{-1}\tau_0)^4\sum_{k=0}^{5} E_k^4 \tau_0^{k+6}, \tag{A10}$$

$$\delta_5 = \lambda(\tau_0^2-1)\sum_{k=0}^{3} E_k^5 \tau_0^{2k+5}, \tag{A11}$$

k	E_k^0	E_k^1	E_k^2	E_k^3	E_k^4	E_k^5	E_k^6	E_k^7
0	$\frac{435}{128}$	$-\frac{245}{128}$	$-\frac{155}{128}$	$-\frac{35}{128}$	96	$-\frac{15}{4}$	$-\frac{33}{4}$	$\frac{3}{2}$
1	$-\frac{25\,061}{128}$	$\frac{35\,285}{192}$	0	0	$\frac{3}{2}$	$-\frac{99}{4}$	54	$-\frac{57}{4}$
2	$\frac{26\,907}{64}$	$-\frac{20\,579}{128}$	$\frac{1973}{384}$	$\frac{35}{64}$	0	$\frac{177}{4}$	$-\frac{297}{4}$	—
3	$-\frac{195\,679}{960}$	$-\frac{8061}{32}$	$\frac{15}{4}$	0	$-\frac{63}{4}$	$-\frac{57}{4}$	$\frac{57}{2}$	—
4	$-\frac{24\,539}{384}$	$\frac{208\,931}{1920}$	$-\frac{186\,809}{384}$	$\frac{8535}{128}$	0	—	—	—
5	$\frac{3943}{128}$	$\frac{42\,665}{192}$	$\frac{69}{4}$	$\frac{33}{4}$	$\frac{57}{4}$	—	—	—
6	—	$-\frac{11\,829}{128}$	$\frac{151\,519}{128}$	$\frac{6921}{32}$	—	—	—	—
7	—	—	−90	−54	—	—	—	—
8	—	—	$-\frac{370\,531}{384}$	$-\frac{29\,597}{128}$	—	—	—	—
9	—	—	$\frac{255}{2}$	$\frac{297}{4}$	—	—	—	—
10	—	—	$\frac{270\,489}{640}$	$\frac{2099}{64}$	—	—	—	—
11	—	—	$-\frac{291}{4}$	$-\frac{57}{2}$	—	—	—	—
12	—	—	$-\frac{97\,043}{384}$	$-\frac{3943}{128}$	—	—	—	—
13	—	—	$\frac{57}{4}$	—	—	—	—	—
14	—	—	$\frac{11\,829}{128}$	—	—	—	—	—

Table 2. Values of E_k^i in the constants associated with the B_2 squirming mode given by (A6)–(A13).

$$\delta_6 = \lambda(\tau_0^2 - 1)\coth^{-1}\tau_0 \sum_{k=0}^{3} E_k^6 \tau_0^{2k+6}, \tag{A12}$$

$$\delta_7 = \lambda(\tau_0^2 - 1)^3(\coth^{-1}\tau_0)^2 \sum_{k=0}^{1} E_k^7 \tau_0^{2k+7}, \tag{A13}$$

where the values of E_k^i are given in table 2.

Appendix B

In this appendix, we remark on the effect of an increased magnitude of α on the swimming speed for pushers ($\alpha < 0$) and pullers ($\alpha > 0$) beyond the weakly non-Newtonian regime discussed in the main text. Figure 7 displays results from numerical simulations when $\alpha = 0, \pm 0.5$ and ± 1 for a spheroidal squirmer with eccentricity $e = 0.6$ (figure 7*a*) and $e = 0.9$ (figure 7*b*). These values of eccentricity are chosen to capture the two distinct scenarios when a neutral spheroidal squirmer ($\alpha = 0$) could swim slower ($e = 0.6$; figure 7*a*) and faster ($e = 0.9$; figure 7*b*) than its Newtonian speed in a shear-thinning fluid. In both cases, the qualitative behaviours of increasing the magnitude of α are similar. First, the asymptotic result (4.1) predicts that the swimming speed is independent of the sign of α at small Cu. Consistent with the asymptotic result, pushers and pullers have the same swimming speeds in a shear-thinning fluid even beyond the asymptotic regime, when

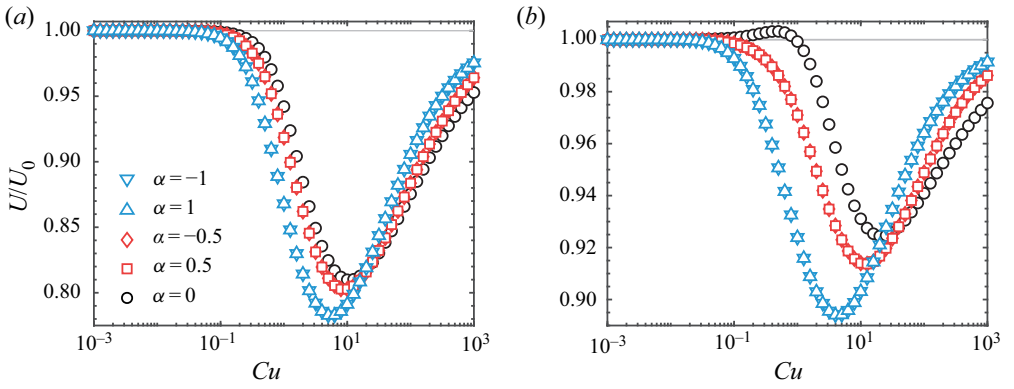

Figure 7. Swimming speed of a spheroidal squirmer U in a shear-thinning fluid relative to its corresponding Newtonian value U_0 for different values of α when (*a*) $e = 0.6$ and (*b*) $e = 0.9$. Consistent with the asymptotic results, numerical simulations here show that pushers ($\alpha < 0$) and pullers ($\alpha > 0$) have indistinguishable swimming speeds in a shear-thinning fluid. In both (*a*,*b*), $n = 0.25$ and $\beta = 0.1$.

the shear-thinning effect becomes more substantial. Second, the swimming speed decays generally with an increased magnitude of α in the small Cu regime, as the asymptotic analysis suggests. More complex variations with α occur at larger values of Cu, and the speed can grow with the magnitude of α; nevertheless, the speed is still smaller than the corresponding value in a Newtonian fluid. Overall, an increased magnitude of α is found to reduce the local minimum speeds in both figures 7(*a*) and 7(*b*), as well as the local maximum speed that appears when $\alpha = 0$ in figure 7(*b*).

References

Bente, K., Codutti, A., Bachmann, F. & Faivre, D. 2018 Biohybrid and bioinspired magnetic microswimmers. *Small* **14**, 1704374.

Binagia, J.P., Phoa, A., Housiadas, K.D. & Shaqfeh, E.S.G. 2020 Swimming with swirl in a viscoelastic fluid. *J. Fluid Mech.* **900**, A4.

Bird, R.B., Armstrong, R.C. & Hassanger, O. 1987 *Dynamics of Polymeric Liquids*, vol. 1. John Wiley.

Blake, J.R 1971 A spherical envelope approach to ciliary propulsion. *J. Fluid Mech.* **46**, 199–208.

Chisholm, N.G., Legendre, D., Lauga, E. & Khair, A.S. 2016 A squirmer across Reynolds numbers. *J. Fluid Mech.* **796**, 233–256.

Cichos, F., Gustavsson, K., Mehlig, B. & Volpe, G. 2020 Machine learning for active matter. *Nat. Mach. Intell.* **2** (2), 94–103.

Colabrese, S., Gustavsson, K., Celani, A. & Biferale, L. 2017 Flow navigation by smart microswimmers via reinforcement learning. *Phys. Rev. Lett.* **118**, 158004.

Daddi-Moussa-Ider, A., Nasouri, B., Vilfan, A. & Golestanian, R. 2021 Optimal swimmers can be pullers, pushers or neutral depending on the shape. *J. Fluid Mech.* **922**, R5.

Datt, C., Zhu, L., Elfring, G.J. & Pak, O.S. 2015 Squirming through shear-thinning fluids. *J. Fluid Mech.* **784**, R1.

De Corato, M., Greco, F. & Maffettone, P.L. 2015 Locomotion of a microorganism in weakly viscoelastic liquids. *Phys. Rev.* E **92**, 053008.

Demir, E., Lordi, N., Ding, Y. & Pak, O.S. 2020 Nonlocal shear-thinning effects substantially enhance helical propulsion. *Phys. Rev. Fluids* **5**, 111301.

Drescher, K., Leptos, K.C., Tuval, I., Ishikawa, T., Pedley, T.J. & Goldstein, R.E. 2009 Dancing *Volvox*: hydrodynamic bound states of swimming algae. *Phys. Rev. Lett.* **102**, 168101.

Eastham, P.S. & Shoele, K. 2020 Axisymmetric squirmers in Stokes fluid with nonuniform viscosity. *Phys. Rev. Fluids* **5**, 063102.

Elfring, G.J. 2017 Force moments of an active particle in a complex fluid. *J. Fluid Mech.* **829**, R3.

Elfring, G.J. & Lauga, E. 2015 Theory of locomotion through complex fluids. In *Complex Fluids in Biological Systems* (ed. S.E. Spagnolie), pp. 283–317. Springer.

ELGETI, J., WINKLER, R.G. & GOMPPER, G. 2015 Physics of microswimmers – single particle motion and collective behavior: a review. *Rep. Prog. Phys.* **78**, 056601.
FAUCI, L.J. & DILLON, R. 2006 Biofluidmechanics of reproduction. *Annu. Rev. Fluid Mech.* **38**, 371–394.
FU, S., WEI, F., YIN, C., YAO, L. & WANG, Y. 2021 Biomimetic soft micro-swimmers: from actuation mechanisms to applications. *Biomed. Microdevices* **23**, 2007403.
GAGNON, D.A. & ARRATIA, P.E. 2016 The cost of swimming in generalized Newtonian fluids: experiments with *C. elegans*. *J. Fluid Mech.* **800**, 753–765.
GAGNON, D.A., KEIM, N.C. & ARRATIA, P.E. 2014 Undulatory swimming in shear-thinning fluids: experiments with *C. elegans*. *J. Fluid Mech.* **758**, R3.
GHOSE, S. & ADHIKARI, R. 2014 Irreducible representations of oscillatory and swirling flows in active soft matter. *Phys. Rev. Lett.* **112**, 118102.
GOLDSTEIN, R.E. 2015 Green algae as model organisms for biological fluid dynamics. *Annu. Rev. Fluid Mech.* **47**, 343–375.
GÓMEZ, S., GODÍNEZ, F.A., LAUGA, E. & ZENIT, R. 2017 Helical propulsion in shear-thinning fluids. *J. Fluid Mech.* **812**, R3.
GUO, H., ZHU, H., LIU, R., BONNET, M. & VEERAPANENI, S. 2021 Optimal slip velocities of micro-swimmers with arbitrary axisymmetric shapes. *J. Fluid Mech.* **910**, A26.
HAN, K., SHIELDS IV, C.W., BHARTI, B., ARRATIA, P.E. & VELEV, O.D. 2020 Active reversible swimming of magnetically assembled 'microscallops' in non-Newtonian fluids. *Langmuir* **36**, 7148–7154.
HAPPEL, J. & BRENNER, H. 1965 *Low Reynolds Number Hydrodynamics*. Prentice Hall Inc.
HARTL, B., HÜBL, M., KAHL, G. & ZÖTTL, A. 2021 Microswimmers learning chemotaxis with genetic algorithms. *Proc. Natl Acad. Sci. USA* **118** (19), e2019683118.
HOUSIADAS, K.D. 2021 An active body in a Phan-Thien and Tanner fluid: the effect of the third polar squirming mode. *Phys. Fluids* **33** (4), 043110.
HOUSIADAS, K.D., BINAGIA, J.P. & SHAQFEH, E.S.G. 2021 Squirmers with swirl at low Weissenberg number. *J. Fluid Mech.* **911**, A16.
HU, C., PANÉ, S. & NELSON, B.J. 2018 Soft micro- and nanorobotics. *Annu. Rev. Control Robot. Auton. Syst.* **1**, 53–75.
HWANG, S.H., LITT, M. & FORSMAN, W.C. 1969 Rheological properties of mucus. *Rheol. Acta* **8**, 438–448.
ISHIKAWA, T. & PEDLEY, T.J. 2007 Diffusion of swimming model micro-organisms in a semi-dilute suspension. *J. Fluid Mech.* **588**, 437–462.
ISHIKAWA, T., SIMMONDS, M.P. & PEDLEY, T.J. 2006 Hydrodynamic interaction of two swimming model micro-organisms. *J. Fluid Mech.* **568**, 119–160.
ISHIKAWA, T., SIMMONDS, M.P. & PEDLEY, T.J. 2007 The rheology of a semi-dilute suspension of swimming model micro-organisms. *J. Fluid Mech.* **588**, 399–435.
ISHIMOTO, K. & GAFFNEY, E.A. 2013 Squirmer dynamics near a boundary. *Phys. Rev.* E **88**, 062702.
KELLER, S.R. & WU, T.Y. 1977 A porous prolate-spheriodal model for ciliated micro-organisms. *J. Fluid Mech.* **80**, 259–278.
LAUGA, E. 2014 Locomotion in complex fluids: integral theorems. *Phys. Fluids* **26**, 081902.
LAUGA, E. 2015 The bearable gooeyness of swimming. *J. Fluid Mech.* **762**, 1–4.
LAUGA, E. 2016 Bacterial hydrodynamics. *Annu. Rev. Fluid Mech.* **48**, 105–130.
LAUGA, E. & POWERS, T.R. 2009 The hydrodynamics of swimming microorganisms. *Rep. Prog. Phys.* **72** (9), 096601.
LI, G. & ARDEKANI, A.M. 2015 Undulatory swimming in non-Newtonian fluids. *J. Fluid Mech.* **784**, R4.
LI, G., LAUGA, E. & ARDEKANI, A.M. 2021 Microswimming in viscoelastic fluids. *J. Non-Newtonian Fluid Mech.* **297**, 104655.
LI, J., ESTEBAN-FERNÁNDEZ DE ÁVILA, B., GAO, W., ZHANG, L. & WANG, J. 2017 Micro/nanorobots for biomedicine: delivery, surgery, sensing, and detoxification. *Sci. Robot.* **2**, eaam6431.
LIGHTHILL, J. 1975 *Mathematical Biofluiddynamics*. SIAM.
LIGHTHILL, M.J. 1952 On the squirming motion of nearly spherical deformable bodies through liquids at very small Reynolds numbers. *Commun. Pure Appl. Maths* **5**, 109–118.
LIU, Y., ZOU, Z., TSANG, A.C.H., PAK, O.S. & YOUNG, Y.-N. 2021 Mechanical rotation at low Reynolds number via reinforcement learning. *Phys. Fluids* **33** (6), 062007.
MAGAR, V., GOTO, T. & PEDLEY, T.J. 2003 Nutrient uptake by a self-propelled steady squirmer. *Q. J. Mech. Appl. Maths* **56**, 65–91.
MAGAR, V. & PEDLEY, T.J. 2005 Average nutrient uptake by a self-propelled unsteady squirmer. *J. Fluid Mech.* **539**, 93–112.
MASOUD, H. & STONE, H.A. 2019 The reciprocal theorem in fluid dynamics and transport phenomena. *J. Fluid Mech.* **879**, P1.

MICHELIN, S. & LAUGA, E. 2010 Efficiency optimization and symmetry-breaking in a model of ciliary locomotion. *Phys. Fluids* **22**, 111901.
MICHELIN, S. & LAUGA, E. 2011 Optimal feeding is optimal swimming for all Péclet numbers. *Phys. Fluids* **23**, 101901.
MONTENEGRO-JOHNSON, T.D. 2017 Fake μs: a cautionary tail of shear-thinning locomotion. *Phys. Rev. Fluids* **2**, 081101.
MONTENEGRO-JOHNSON, T.D., SMITH, D.J. & LOGHIN, D. 2013 Physics of rheologically enhanced propulsion: different strokes in generalized Stokes. *Phys. Fluids* **25** (8), 081903.
MORAN, J.L. & POSNER, J.D. 2017 Phoretic self-propulsion. *Annu. Rev. Fluid Mech.* **49** (1), 511–540.
MUIÑOS-LANDIN, S., FISCHER, A., HOLUBEC, V. & CICHOS, F. 2021 Reinforcement learning with artificial microswimmers. *Sci. Robot.* **6** (52), eabd9285.
NELSON, B.J., KALIAKATSOS, I.K. & ABBOTT, J.J. 2010 Microrobots for minimally invasive medicine. *Annu. Rev. Biomed. Engng* **12** (1), 55–85.
NGANGUIA, H., PIETRZYK, K. & PAK, O.S. 2017 Swimming efficiency in a shear-thinning fluid. *Phys. Rev.* E **96** (6), 062606.
NGANGUIA, H., ZHENG, K., CHEN, Y., PAK, O.S. & ZHU, L. 2020 A note on a swirling squirmer in a shear-thinning fluid. *Phys. Fluids* **32**, 111906.
PAK, O.S. & LAUGA, E. 2014 Generalized squirming motion of a sphere. *J. Engng Maths* **88**, 1–28.
PEDLEY, T.J. 2016 Spherical squirmers: models for swimming micro-organisms. *IMA J. Appl. Maths* **81**, 488–521.
PEDLEY, T.J., BRUMLEY, D.R. & GOLDSTEIN, R.E. 2016 Squirmers with swirl: a model for *Volvox* swimming. *J. Fluid Mech.* **798**, 165–186.
PIETRZYK, K., NGANGUIA, H., DATT, C., ZHU, L., ELFRING, G.J. & PAK, O.S. 2019 Flow around a squirmer in a shear-thinning fluid. *J. Non-Newtonian Fluid Mech.* **268**, 101–110.
PÖHNL, R., POPESCU, M. & USPAL, W. 2020 Axisymmetric spheroidal squirmers and self-diffusionphoretic particles. *J. Phys.: Condens. Matter* **32**, 164001.
QIU, T., LEE, T.-C., MARK, A.G., MOROZOV, K.I., MÜNSTER, R., MIERKA, O., TUREK, S., LESHANSKY, A.M. & FISCHER, P. 2014 Swimming by reciprocal motion at low Reynolds number. *Nat. Commun.* **5**, 5119.
QU, Z. & BREUER, K.S. 2020 Effects of shear-thinning viscosity and viscoelastic stresses on flagellated bacteria motility. *Phys. Rev. Fluids* **5**, 073103.
REIGH, S.Y. & LAUGA, E. 2017 Two-fluid model for locomotion under self-confinement. *Phys. Rev. Fluids* **2**, 093101.
RILEY, E.E. & LAUGA, E. 2017 Empirical resistive-force theory for slender biological filaments in shear-thinning fluids. *Phys. Rev.* E **95**, 062416.
SCHNEIDER, E. & STARK, H. 2019 Optimal steering of a smart active particle. *Europhys. Lett.* **127** (6), 64003.
SENGUPTA, S., IBELE, M.E. & SEN, A. 2012 Fantastic voyage: designing self-powered nanorobots. *Angew. Chem. Intl Ed. Engl.* **51**, 8434–8445.
STONE, H.A. & SAMUEL, A.D.T. 1996 Propulsion of microorganisms by surface distortions. *Phys. Rev. Lett.* **77**, 4102–4104.
SZNITMAN, J. & ARRATIA, P.E. 2015 Locomotion through complex fluids: an experimental view. In *Complex Fluids in Biological Systems* (ed. S.E. Spagnolie), pp. 245–281. Springer.
THEERS, M., WESTPHAL, E., GOMPPER, G. & WINKLER, R.G. 2016 Modeling a spheroidal microswimmer and cooperative swimming in a narrow slit. *Soft Matt.* **12**, 7372–7385.
TSANG, A.C.H., DEMIR, E., DING, Y. & PAK, O.S. 2020*a* Roads to smart artificial microswimmers. *Adv. Intell. Syst.* **2**, 1900137.
TSANG, A.C.H., TONG, P.W., NALLAN, S. & PAK, O.S. 2020*b* Self-learning how to swim at low Reynolds number. *Phys. Rev. Fluids* **5**, 074101.
VÉLEZ-CORDERO, J.R. & LAUGA, E. 2013 Waving transport and propulsion in a generalized Newtonian fluid. *J. Non-Newtonian Fluid Mech.* **199**, 37–50.
WANG, S. & ARDEKANI, A. 2012 Inertial squirmer. *Phys. Fluids* **24** (10), 101902.
WU, Z., CHEN, Y., MUKASA, D., PAK, O.S. & GAO, W. 2020 Medical micro/nanorobots in complex media. *Chem. Soc. Rev.* **49**, 8088–8112.
YEOMANS, J.M., PUSHKIN, D.O. & SHUM, H. 2014 An introduction to the hydrodynamics of swimming microorganisms. *Eur. Phys.* J.*: Spec. Top.* **223**, 1771–1785.
ZHU, L., DO-QUANG, M., LAUGA, E. & BRANDT, L. 2011 Locomotion by tangential deformation in a polymeric fluid. *Phys. Rev.* E **83**, 011901.
ZHU, L., LAUGA, E. & BRANDT, L. 2012 Self-propulsion in viscoelastic fluids: pushers vs pullers. *Phys. Fluids* **24**, 051902.